INL/EXT-17-43135 Rev. 0

August 2017

Lower length scale modeling of Cr precipitation in FeCrAl under thermal aging conditions

Chao Jiang
Yongfeng Zhang
Enrique Martinez (LANL)

INL/EXT-17-43135 Rev. 0

Lower length scale modeling of Cr precipitation in FeCrAl under thermal aging conditions

Chao Jiang
Yongfeng Zhang
Enrique Martinez (LANL)

August 2017

Idaho National Laboratory
Fuel Modeling and Simulation Department
Idaho Falls, Idaho 83415

Prepared for the
U.S. Department of Energy
Office of Nuclear Energy
Under U.S. Department of Energy-Idaho Operations Office
Contract DE-AC07-99ID13727

ABSTRACT

This report summarizes the progress on lower length scale modeling of Cr precipitation in FeCrAl alloys, which has been identified as a possible cladding material for accident tolerant fuels due to its excellent corrosion resistance via the formation of a protective, slow growing alumina surface layer. The precipitation of Cr-rich α' clusters in FeCrAl can lead to degraded mechanical properties such as the well-known "475°C embrittlement", and should therefore be avoided to ensure cladding integrity. In FY16, a lattice kinetic Monte Carlo (LKMC) model was developed for FeCr binary alloys. Due to the assumption of constant bond energies, the previous model cannot correctly reproduce the low-temperature part of the Fe-Cr phase diagram. It is also not possible to model the anomalous ordering tendency and repulsive interactions between Cr atoms in α Fe at the dilute concentration regime using constant bond energies. To address these issues, a new local-environment-dependent bond energy formalism has been developed for Fe-Cr in FY17 that can simultaneously reproduce the negative mixing energy at low Cr concentrations and the positive mixing energy at high Cr concentrations, and the consequent large solubility of Cr in bcc Fe at low temperatures. Furthermore, the LKMC model has been extended to include Al to enable the assessment of Cr precipitation tendency in ternary FeCrAl alloys under thermal aging. Results from the present KMC simulations show good agreement with available experiments in the literature. This study is supported by the DOE NEAMS program Accident Tolerant Fuel project.

CONTENTS

FIGURES

1 Introduction

Fe-Cr-Al alloys with high Cr content (10-25wt%) and up to 5wt% Al have been recently proposed as candidate accident tolerant fuel (ATF) cladding materials due to their excellent resistance to water corrosion (oxidation), and consequent reduction of heat and hydrogen generation during severe accidents [1]. The good corrosion resistance originates from the high Cr concentration and the protective, slow-growing Al oxide layer formed at the surface. Under neutron irradiation, the corrosion resistance of Fe-Cr-Al alloys can be degraded due to the precipitation of Cr-rich α' phase, which will deplete the Cr content in the matrix. α' precipitates can also hinder dislocation motion, leading to hardening and embrittlement. Note that, at the cladding operating temperature ($\sim$300-400°C), the precipitation process can be drastically accelerated under neutron irradiation due to radiation-enhanced-diffusion. While the irradiation effects have been extensively studied for Fe-Cr alloys, it is not clear how Al addition will change the α' precipitation, calling for mechanistic understanding from both modeling and experimental sides. In FY17, a local-environment-dependent bond energy formalism has been developed for bcc Fe-Cr-Al alloys and parameterized using ab initio density functional theory (DFT) calculations. The local-environment-dependent bond energy model is subsequently employed to calculate phase diagrams and to drive kinetic Monte-Carlo simulations of α' precipitation in bcc Fe-Cr-Al alloys. The modeling methodology and results are summarized in this report.

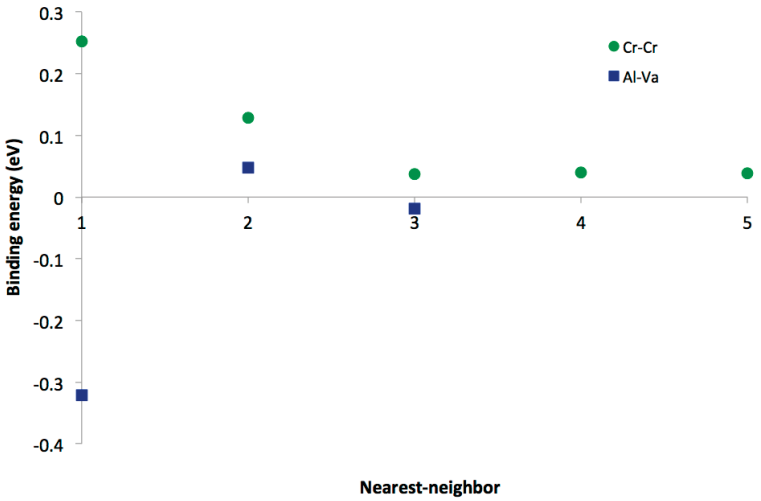

Figure 1: DFT calculated Cr-Cr and Al-vacancy binding energies (in eV) in a 128-atom pure bcc Fe supercell. A positive binding energy indicates repulsion between the two entities considered, and vice versa.

2 Model development

2.1 DFT calculations

For the parameterization of the LKMC model for FeCrAl, we have performed ab initio calculations using the all-electron projector augmented wave method within the generalized gradient approximation of Perdew, Burke, and Ernzerhof (PBE-GGA) [2], as implemented in the Vienna ab initio simulation package (VASP) code [3]. The plane-wave cut-off energy is set at 350 eV. The k-point meshes for Brillouin zone sampling are constructed using the MonkhorstPack scheme and the total number of k-points times the total number of atoms per unit cell was at least 5000 for all structures. These settings ensure high numerical accuracy for total energy calculations. In our previous study [4], DFT calculations have been used to directly obtain the total energy change due to a vacancy jump in random Fe-Cr and Fe-Al alloys. By fitting to the DFT calculated ΔE values, the bond energies for Fe-Cr and Fe-Al systems were parameterized.

In this work, we further use DFT to calculate the Cr-Cr and Al-vacancy binding energies in pure bcc Fe and the mixing energies of random bcc Fe-Cr alloys, and the results are shown in Figures 1 and 2. In addition to revealing very strong binding between Al and vacancy in bcc Fe matrix, Figure 1 indicates strong repulsion between Cr atoms at dilute concentrations. This finding is interesting since Cr atoms are known to have a strong clustering tendency at high Cr concentrations, leading to the formation of a miscibility gap in the Fe-Cr system [5]. It can also be observed from Figure 2 that the mixing energy curve for Fe-Cr is strongly non-symmetric and even becomes negative at small Cr concentrations. Due to the negative mixing energy, the solubility of Cr in Fe can remain large even at low temperatures. In order to reproduce these anomalous features of the Fe-Cr system, it is necessary to use a local-environment-dependent bond energy model, which will be discussed in the next section.

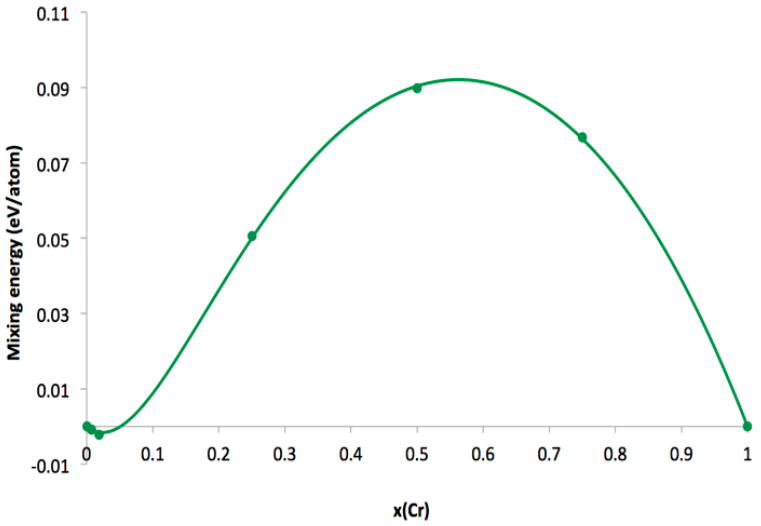

Figure 2: DFT calculated mixing energies of random Fe-Cr alloys at 0 K.

2.2 KMC simulations

For kinetic Monte Carlo (KMC) simulations of Cr precipitation in bcc FeCrAl, we employ the rejection-free residence time algorithm and transition state theory widely used in the literature for studying the precipitation of solute elements in bcc Fe under both thermal aging and irradiation conditions [6, 7, 8, 9, 10, 11]. A vacancy-mediated diffusion mechanism is assumed, which is valid for thermal aging conditions considered in this report. Note that, under irradiation, diffusion of chemical species can be greatly accelerated due to super-saturation of point defects (vacancies and interstitials) created by collision cascades, which is called radiation-enhanced diffusion. Diffusion of interstitials or vacancies towards defect sinks can also lead to redistribution of solute concentrations, so-called radiation-induced segregation. For simplicity, such effects are not considered in this work.

For vacancy diffusion on a bcc lattice, a vacancy can jump to one of its eight first-nearest-neighbor (1NN) sites with jump rate:

$$\Gamma_{X\to V} = \nu_X \exp\left(-\frac{E^{mig}_{X\to V}}{k_B T}\right) \tag{1}$$

where ν_X is the attempt frequency of the atom X exchanging position with the vacancy, $E^{mig}_{X\to V}$ is the migration barrier of the X→V jump, and k_B is Boltzmann's constant. Second-nearest-neighbor (2NN) vacancy jumps are neglected due to their higher barriers. Out of eight possible jump events, one is selected by a random number and the average residence time is given by:

$$t_{MC} = \left(\sum_{i=1}^{8} \Gamma_i\right)^{-1} \tag{2}$$

Since the vacancy concentration in KMC simulations (c_V^{sim}) can be significantly greater than the equilibrium vacancy concentration (c_V^{eq}) in the alloy, the physical time is advanced by proper rescaling of the KMC time:

$$t = t_{MC}\left(\frac{c_V^{sim}}{c_V^{eq}}\right) \tag{3}$$

One of the most important ingredient of a KMC model is the determination of local-environment-dependent vacancy migration barrier, $E^{mig}_{X\rightarrow V}$, which can be estimated from the final and initial system energy (FISE) [11] as:

$$E^{mig}_{X\rightarrow V} = E^{mig}_{X} + \Delta E/2 \tag{4}$$

where $E^{mig}_{X\rightarrow V}$ is the migration barrier for $X \rightarrow V$ jump in pure bcc Fe. By performing climbing image nudged elastic band (CI-NEB) calculations [12] as implemented in VASP, the values of E^{mig}_{Fe}, E^{mig}_{Cr} and E^{mig}_{Al} are obtained to be 0.691 eV, 0.57 eV and 0.487 eV, respectively. $\Delta E = E_f - E_i$ is the energy difference before and after the vacancy jump, which can either directly calculated from an empirical interatomic potential, or can be estimated using the pair interaction model. In this work, based on the observation that Cr atoms actually strongly repel each other at dilute concentrations (see Figure 1) despite their clustering tendency at high Cr concentrations, we have developed a local-environment-dependent bond energy model for FeCrAl. Our design philosophy is to separate the total energy into a summation of local-environment-independent and local-environment-dependent contributions. For the local-environment-independent part of the total energy, we can simply reuse the constant bond energies from our previous work [4]. Only the local-environment-dependent contributions, completely neglected in our previous work, need to be parameterized. According to this model, the total energy E of a system can be estimated as follows:

$$E = \frac{1}{2}\sum_{i=1}^{4}\sum_{j=1}^{4} n^{1NN}_{i-j}\varepsilon^{1NN}_{i-j} + \frac{1}{2}\sum_{i=1}^{4}\sum_{j=1}^{4} n^{2NN}_{i-j}\varepsilon^{2NN}_{i-j} + E_{local1} - E_{local2} \tag{5}$$

where ε_{i-j} is the energy of a first-nearest-neighbor (1NN) or second-nearest-neighbor (2NN) bond of type i-j, and is assumed to be a constant. n_{i-j} is the number of bonds of type i-j. Here $i(j)$=1,2,3,4 denotes Fe, Cr, Al and vacancy, respectively. In practice, the bond energies ε^{1NN}_{i-j} and ε^{2NN}_{V-i} can be fitted to experimental or theoretical data such as the cohesive energies and vacancy formation energies of pure elements, the solution energies of solutes in bcc Fe, the mixing energies of random alloys, the solute-solute and solute-vacancy binding energies, often with the additional assumption that $\varepsilon^{2NN}_{i-j} = \frac{1}{2}\varepsilon^{1NN}_{i-j}$ [7, 9].

E_{local1} is the contribution due to local-environment-dependent interactions between a Cr atom and its neighboring Cr atoms up to fifth-nearest-neighbor (5NN) separation and can be generally written as:

$$E_{local1} = \frac{1}{2}\sum_{k=1}^{5}\sum_{i=Cr}\sum_{j\in kNN(i),j=Cr} f_i f_j e^{kNN}_{Cr-Cr} \tag{6}$$

Here the summation goes over all Cr-Cr pairs up to 5NN interaction. f_i and f_j characterize the local environment of Cr atoms at lattice site i and j, respectively. When a Cr atom is surrounded by a nearly pure Fe environment, factor f will approach one. Conversely, when a Cr atom is surrounded by many other Cr atoms, factor f will approach zero.

In the simplest case, f_i can be written as a linear function of the number of near-neighbor Cr atoms surrounding a Cr atom at site i as:

$$f_i = 1 - \sum_{k=1}^{5} w_k n^k_i \tag{7}$$

Here n^k_i is the number of Cr atoms in the kNN shell of a Cr atom at site i. w_k is a weight factor indicating the influence of Cr atoms in the kNN shell and its value should rapidly decrease to zero

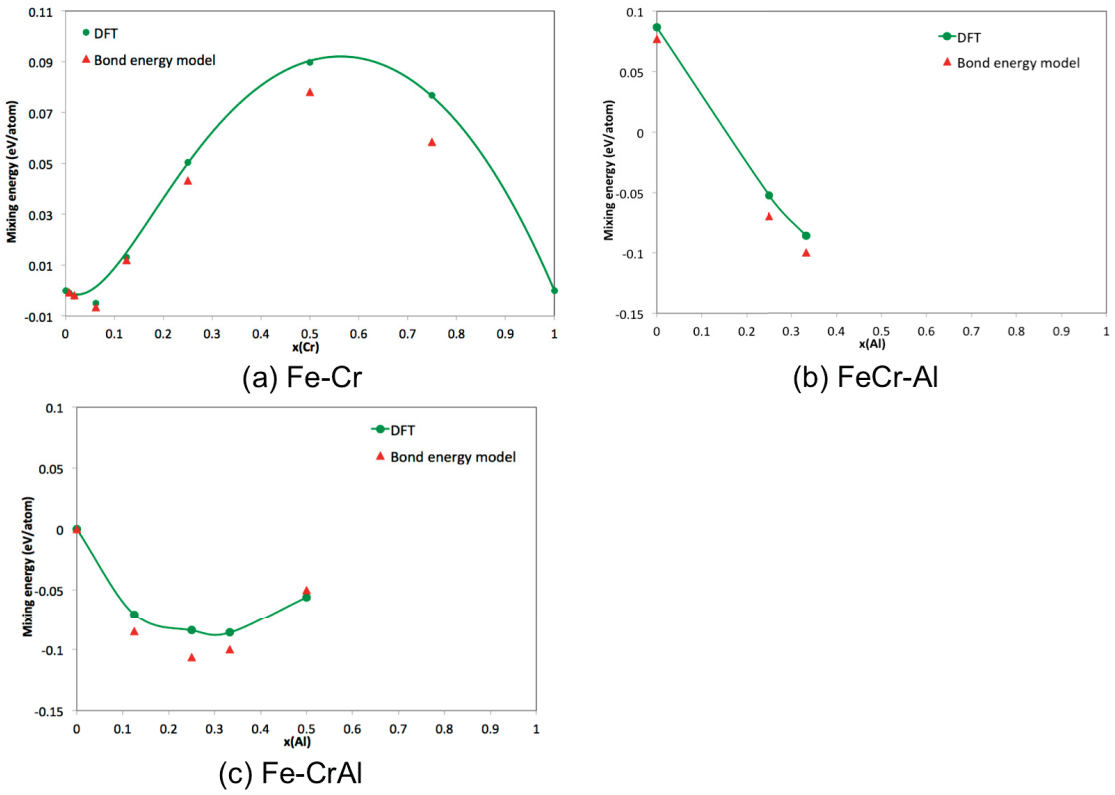

Figure 3: Comparison between bond energy calculated and DFT calculated mixing energies of Fe-Cr and Fe-Cr-Al alloys. The solids lines are drawn to guide the eye.

with increasing k. e^{kNN}_{Cr-Cr} represents the repulsion energy between two Cr atoms in pure Fe at the kNN separation, whose values can be derived from the DFT data reported in Figure 1.

Finally, E_{local2} is used to model the negative mixing energies of Fe-Cr alloys at dilute Cr concentrations:

$$E_{local2} = \sum_{k=1}^{2} \sum_{i=Cr} \sum_{j \in kNN(i), j=Fe} f_i e^{kNN}_{Fe-Cr} \tag{8}$$

The summation goes over all Cr-Fe pairs up to 2NN interaction. Here, the values of e^{kNN}_{Fe-Cr} are fitted to the DFT calculated mixing energies in Figure 2.

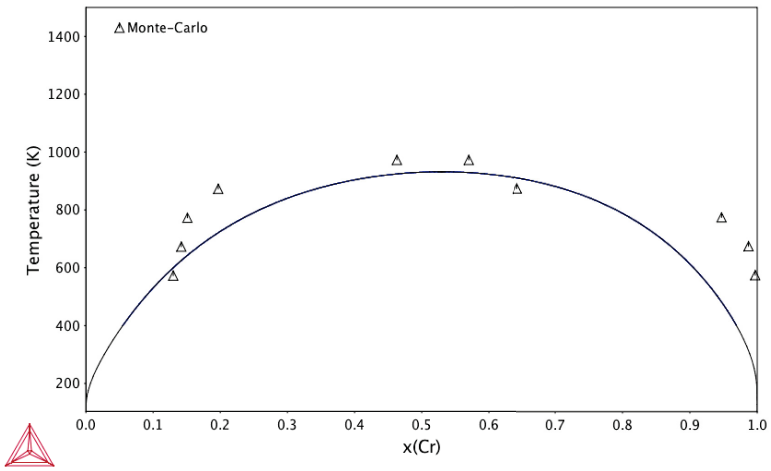

Figure 4: Comparison between Monte-Carlo calculated and CALPHAD predicted bcc miscibility gap in the Fe-Cr binary system.

3 Results and discussion

3.1 Thermodynamic calculations

It is well known that thermodynamics dictates the final equilibrium state of a system, while kinetics controls how fast the equilibrium state can be reached. It is thus critical to first validate the accuracy of the developed local-environment-dependent bond energy model in representing the thermodynamics of the Fe-Cr-Al system. To this end, we first compare the bond energy model predicted mixing energies of bcc FeCr and FeCrAl alloys with those predicted by DFT. As shown in Figure 3, the agreement is excellent, which is as expected since the bond energy model is parameterized by DFT.

As a more stringent test, the current local-environment-dependent bond energy model has been used to drive Monte-Carlo simulations to predict the miscibility gap in binary Fe-Cr and ternary Fe-Cr-Al systems. As shown in Figures 4 and 5, the Monte-Carlo predicted phase diagrams show very good agreement with those calculated by Thermo-Calc software with thermodynamic parameters assessed using the CALPHAD approach [5]. The only discrepancy is that the CALPHAD-predicted equilibrium Cr concentration of the α' phase is lower than that predicted by current Monte-Carlo simulations. At 773 K, CALPHAD and current model predict the Cr concentration of α' to be 0.81 and 0.95, respectively. Detailed 3D atom probe tomography (APT) experiments may be used to resolve such a discrepancy.

3.2 KMC simulation of FeCr

Figure 6 show the results from KMC simulations of binary Fe-20Cr alloy using the present local-environment-dependent bond energy model. Initially, all Cr atoms are randomly distributed, i.e., with zero Cowley-Warren short-range order (SRO). Here the SRO parameter for an A-B binary alloy is defined as:

$$\alpha^{kNN} = 1 - \frac{p_A^{B,kNN}}{x_B} = 1 - \frac{p_B^{A,kNN}}{1 - x_B} \tag{9}$$

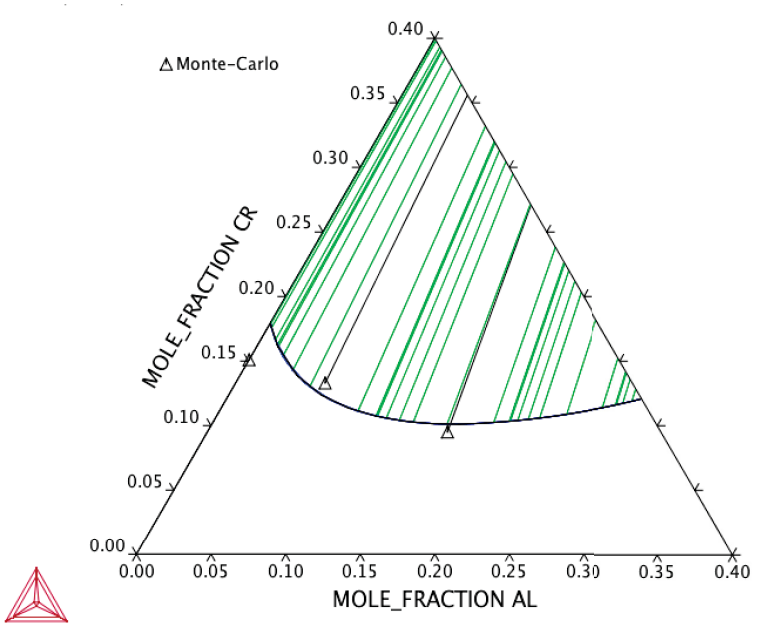

Figure 5: Comparison between Monte-Carlo calculated (triangles) and CALPHAD predicted (solid lines) bcc miscibility gap in the Fe-Cr-Al ternary system at 500°C.

where $p_A^{B,kNN}$ is the probability of finding a B atom in the kNN shell of a A atom. A positive α value means phase separation tendency. The largest possible value of α is 1, which corresponds to the fully segregated state. An α value close to zero means random mixing of A and B atoms. Finally, a negative α value means ordering tendency.

From Figure 6(c), it can be seen that the SRO parameter of the Fe-20Cr alloy initially rapidly increases with time, which is due to the nucleation and growth of α' particles. For longer time (>2000 hours), the curve becomes almost flat, indicating the coarsening stage when small α' particles grow into bigger ones. After 5000 hours of thermal aging, a large α' cluster containing 5619 atoms (1557 Fe atoms and 4062 Cr atoms) is formed near the center of the simulation cell (see Figure 6(a)). The cross-section of this cluster is further shown in Figure 6(b). Based on the number of Fe and Cr atoms, the Cr concentration of this cluster is calculated to be 0.712, which is much lower than the value (0.828) determined by the 3D-APT experiments of Novy et al.[13]. There can be several reasons for this apparent discrepancy. First. as was pointed out by Martinez et al.[9], the spatial resolution of APT may be limited by aberrations of ion trajectories. The choice of parameters in identifying solute clusters can introduce further uncertainty. In contrast, the matrix concentration is much less sensitive to such uncertainties. From the modeling side, the determination of the Cr concentration of α' cluster has its own ambiguity. As can be seen in Figure 6(b), most of the 1557 Fe atoms (shown as yellow spheres) are actually located on the surface of the α' cluster, not interior. It is therefore more reasonable to treat these peripheral Fe atoms as belonging to the α matrix surrounding the cluster, and do not consider them in calculating the Cr concentration of the α' cluster. Indeed, after this correction is made, the agreement between modeling and experiments is excellent for both the concentrations of α and α' (see Figure 6(d)). It is worth noting that, during the measurement of the concentrations of small α' precipitates, some contribution from the surrounding α matrix is inevitable. Presumably, this explains why the experimental Cr concentration of α' (0.828) is still less than the equilibrium value at 500°C (0.947) determined by our Monte Carlo simulations.

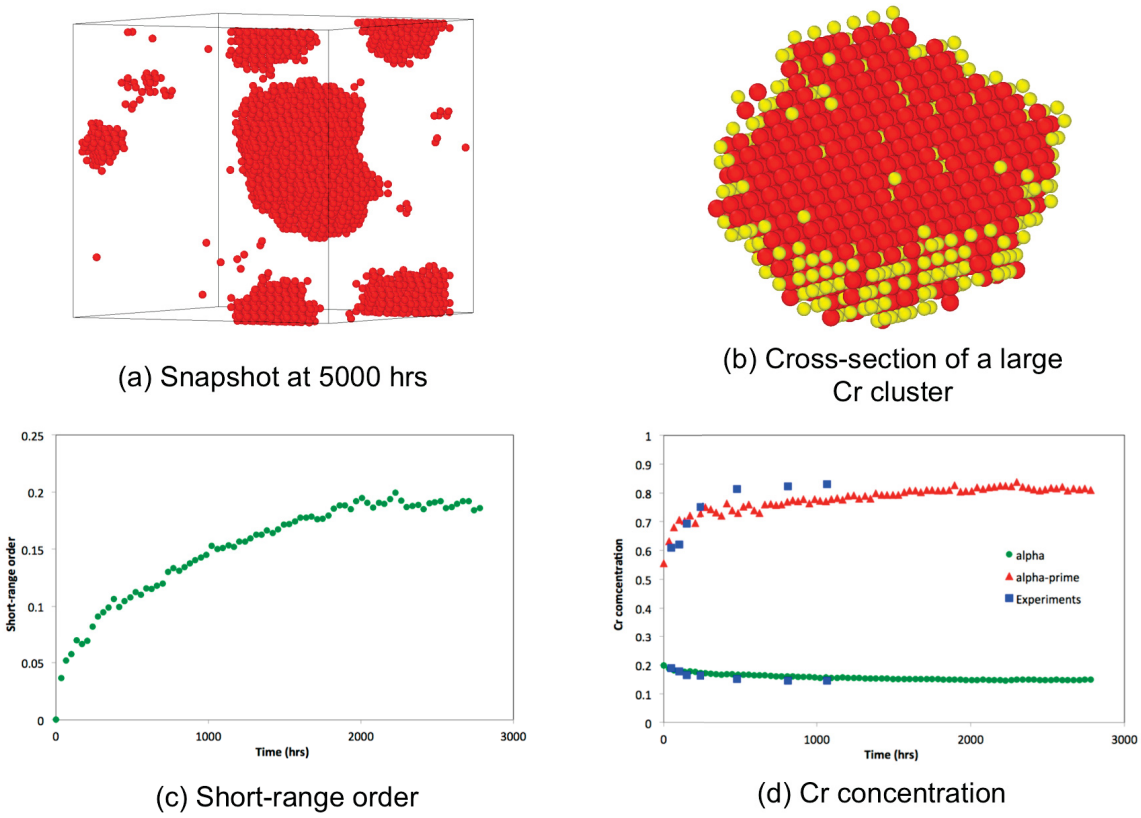

Figure 6: KMC simulation of Cr precipitation in bcc Fe-20Cr alloy at 500°C. Yellow spheres denote Fe atoms. Red spheres denote Cr atoms in α' clusters. Data from APT experiments are also shown for comparison.

3.3 KMC simulation of FeCrAl

Driven by the local-environment-dependent bond energy model developed in this work, KMC simulations have been performed to study α' precipitation in bcc Fe-Cr and Fe-Cr-Al alloys under thermal aging conditions. All simulations start from an initially homogenized simulation cell containing a single vacancy. Diffusion is mediated by the exchange of the vacancy with one of its eight 1NN atoms. In agreement with experiments [14], the present KMC simulations predict no Cr precipitation in Fe-10Cr-8Al alloy and Cr precipitation in Fe-21Cr-10Al at 500°C, as shown in Figure 7. It can be seen that the SRO parameter for Fe-10Cr-8Al alloy quickly reaches its equilibrium value, which is negative due to the ordering of Cr atoms. In contrast, for Fe-21Cr-10Al, the SRO parameter slowly increases with time. The positive SRO is an indication of phase separation. Here, the phase separation process is much slower than ordering since the former requires long-range diffusion of Cr atoms.

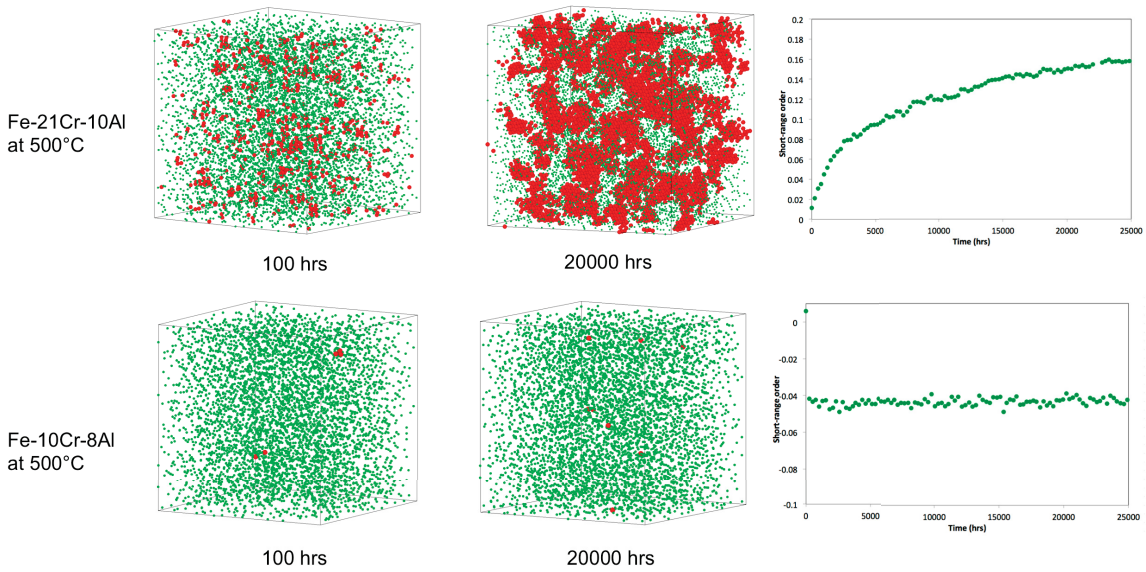

Figure 7: KMC simulation of Cr precipitation in bcc Fe-21Cr-10Al and Fe-10Cr-8Al alloys. Green spheres denote Al atoms. Red spheres denote Cr atoms in α' clusters. For clarity of visualization, all Cr atoms in the solid solutions and all Fe atoms are not shown.

4 Summary

In this work, a new local-environment-dependent bond energy model has been developed for FeCrAl. All parameters of this model are derived by fitting to DFT calculated data such as the total energy change associated with a nearest-neighbor vacancy jump, the binding energy for atom-atom or atom-vacancy interactions, migration barriers for vacancy jump, and the mixing energy of random alloys. This new model can simultaneously describe the ordering tendency (repulsive Cr-Cr interaction) in the dilute solid solution phase and the phase separating tendency (attractive Cr-Cr interactions) at high Cr concentrations in Fe-Cr-based alloys. The Fe-Cr and Fe-Cr-Al phase diagrams predicted by the present model are in good agreement with CALPHAD calculations. Importantly, KMC simulations predict α' precipitation in Fe-21Cr-10Al alloy but not in Fe-10Cr-8Al alloy at 500°C, which is complete agreement with experiments.

5 References

1. Y Zhang, D Schwen, C Jiang, and E Martinez. Literature review report on atomistic modeling tools for fecral alloys. Technical report, Idaho National Laboratory, 2015.

2. JP Perdew, K Burke, and M Ernzerhof. Generalized gradient approximation made simple. *Physical Review Letters*, 77:3865–3868, 1996.

3. G Kresse and J Furthmuller. Efficient iterative schemes for ab initio total-energy calculations using a plane-wave basis set. *Physical Review B*, 54:11169–11186, 1996.

4. Y Zhang, D Schwen, L Aagesen, K Ahmed, J Yu, B Beeler, and C Jiang. Overview of low length scale model development for accident tolerant fuels regarding u3si2 fuel and fecral cladding. Technical report, Idaho National Laboratory, 2016.

5. W Xiong, P Hedstrom, M Selleby, J Odqvist, M Thuvander, and Chen Q. An improved thermodynamic modeling of the fecr system down to zero kelvin coupled with key experiments. *CALPHAD*, 35:355–366, 2011.

6. F Soisson, A Barbu, and G Martin. Monte carlo simulations of copper precipitation in dilute iron-copper alloys during thermal ageing and under electron irradiation. *Acta Materialia*, 44:3789–3800, 1996.

7. S Schmauder and P Binkele. Atomistic computer simulation of the formation of cu-precipitates in steels. *Computational Materals Science*, 24:42–53, 2002.

8. F Soisson and CC Fu. Cu-precipitation kinetics in alpha-fe from atomistic simulations: Vacancy-trapping effects and cu-cluster mobility. *Physical Review B*, 76:214102, 2007.

9. E Martinez, O Senninger, F Soisson, and CC Fu. Decomposition kinetics of fe-cr solid solutions during thermal aging. *Physical Review B*, 86:224109, 2012.

10. F Soisson and T Jourdan. Radiation-accelerated precipitation in fe-cr alloys. *Acta Materialia*, 103:870–881, 2016.

11. E Vincent, CS Becquart, C Pareige, P Pareige, and C Domain. Precipitation of the fecu system: A criticle review of atomic kinetic monte carlo simulations. *Journal of Nuclear Materials*, 373:387–401, 2008.

12. G Henkelman and H Jonsson. A climbing image nudged elastic band method for finding saddle points and minimum energy paths. *Journal of Chemical Physics*, 113:9901–9904, 2000.

13. S Novy, P Pareige, and C Pareige. Atomic scale analysis and phase separation understanding in a thermally aged fe-20 at.% cr alloy. *Journal of Nuclear Materials*, 384:96–102, 2009.

14. J Ejenstam, M Thuvander, P Olsson, F Rave, and P Szakalos. Microstructural stability of fe-cr-al alloys at 450-550°c. *Journal of Nuclear Materials*, 457:291–297, 2015.